Loosely coupled level sets for retinal layers and drusen segmentation in subjects with dry age-related macular degeneration

Novosel, Jelena; Wang, Ziyuan; de Jong, Henk; Vermeer, Koenraad A; van Vliet, Lucas J

DOI
10.1117/12.2214698

Publication date
2016

Document Version
Final published version

Published in
Medical Imaging 2016: Image Processing

Loosely coupled level sets for retinal layers and drusen segmentation in subjects with dry age-related macular degeneration

Jelena Novosel[1,2], Ziyuan Wang[2], Henk de Jong[1], Koenraad A. Vermeer[1], Lucas J. van Vliet[2]
[1]Rotterdam Ophthalmic Institute, Rotterdam Eye Hospital, Rotterdam, The Netherlands,
[2]Department of Imaging Physics, Faculty of Applied Sciences, TU Delft, The Netherlands

ABSTRACT

Optical coherence tomography (OCT) is used to produce high-resolution three-dimensional images of the retina, which permit the investigation of retinal irregularities. In dry age-related macular degeneration (AMD), a chronic eye disease that causes central vision loss, disruptions such as drusen and changes in retinal layer thicknesses occur which could be used as biomarkers for disease monitoring and diagnosis. Due to the topology disrupting pathology, existing segmentation methods often fail. Here, we present a solution for the segmentation of retinal layers in dry AMD subjects by extending our previously presented loosely coupled level sets framework which operates on attenuation coefficients. In eyes affected by AMD, Bruch's membrane becomes visible only below the drusen and our segmentation framework is adapted to delineate such a partially discernible interface. Furthermore, the initialization stage, which tentatively segments five interfaces, is modified to accommodate the appearance of drusen. This stage is based on Dijkstra's algorithm and combines prior knowledge on the shape of the interface, gradient and attenuation coefficient in the newly proposed cost function. This prior knowledge is incorporated by varying the weights for horizontal, diagonal and vertical edges. Finally, quantitative evaluation of the accuracy shows a good agreement between manual and automated segmentation.

Keywords: Optical coherence tomography , attenuation coefficient, Dijkstra's algorithm (up to 8 keywords)

1. INTRODUCTION

Optical coherence tomography (OCT) is a non-invasive imaging technique that produces high-resolution, three-dimensional images of the retina[1] in which pathological irregularities of the retinal structure can be investigated. In dry age-related macular degeneration (AMD), a common sight-threatening disease with an increasing prevalence due to the aging population[2], several changes in the retina occur. First, the inner[3,4], outer[5] and total[6] retinal thicknesses change. Second, drusen (extracellular deposits) occur between the retinal pigment epithelium (RPE) and Bruch's membrane[7,8]. As such, both drusen volumes and thicknesses of various retinal layers are of interest as potential biomarkers for disease monitoring and diagnosis. Since manual segmentation is tedious, time consuming and has poor reproducibility, automatic segmentation of retinal layers and drusen in dry AMD is needed.

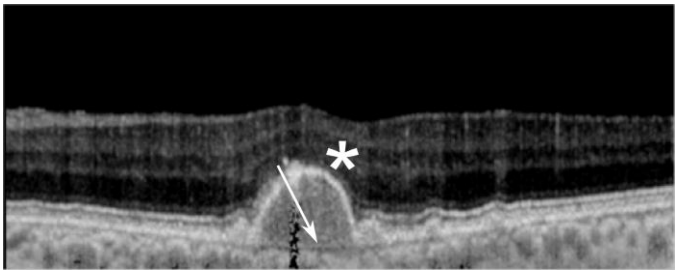

Figure 1. An example of an attenuation coefficient B-scan of an eye affected with dry AMD. The asterisk indicates the elevation of the RPE due to drusen, whereas the arrow indicates Bruch's membrane which becomes visible below the large drusen deposits.

*j.novosel@eyehospital.nl

Medical Imaging 2016: Image Processing, edited by Martin A. Styner, Elsa D. Angelini, Proc. of SPIE Vol. 9784, 97842P · © 2016 SPIE
CCC code: 1605-7422/16/$18 · doi: 10.1117/12.2214698

However, automatic segmentation or retinal layer remains a challenging task in retinas affected by dry AMD as the presence of drusen affects the morphology of the retinal layers. Furthermore, drusen can vary in size, shape and location. Finally, Bruch's membrane, which becomes separated from the RPE, often has a low contrast. Figure 1 shows an example of a B-scan from an eye affected by dry AMD in which some of the segmentation challenges are indicated. So far, existing segmentation approaches focused on the segmentation of the drusen[9,10,11]. These approaches provided segmentation of only three interfaces between the layers: the vitreous – retinal nerve fiber layer (RNFL) interface, the RPE boundary and Bruch membrane. Only a few approaches performed segmentation of multiple layers in the retinas affected by dry AMD[12,13]. However, these approaches either focused on examining retinal layer texture without evaluating the accuracy of the layer segmentation[12] or the retinal layer segmentation was evaluated only on healthy retinas[13]. Finally, Niu et al. reported that their segmentation approach failed in segmenting of retinal layer boundaries in the presence of drusen[14].

Here, we present a method for the segmentation of the retinal layers in dry AMD subjects by extending our previously proposed loosely coupled level sets (LCLS) framework, which was already shown to be accurate on healthy and glaucoma affected eyes[15]. All layers are segmented simultaneously with the coupling strength being based on the incorporated prior knowledge such as the layer order and the expected thickness range. The approach operates on attenuation coefficients, an optical property of the tissue not affected by some common imaging artefacts[16]. Due to pathological changes in the retinal structure that occur in eyes affected by dry AMD, several modifications of our original approach were needed. The first major modification was the introduction of an additional interface which corresponded to Bruch's membrane. This membrane can be challenging to segment, as it is only visible below the drusen and has very low contrast. In areas without drusen, this membrane becomes indiscernible from the RPE boundary. With this additional interface, the presented approach segments eight interfaces. The second major modification was performed in the initialization stage of the approach. The initialization aims to roughly segment five interfaces based on Dijkstra's algorithm[17], however, the cost functions for several interfaces were modified. Some of the added modifications reflect the prior knowledge about the appearance of the layers in dry AMD (e.g. Bruch's membrane is a smooth, almost flat interface, in contrast to the inner segment (IS) boundary which can become irregular and curved due to drusen). This knowledge was incorporated in the cost function by favoring either horizontal, vertical or diagonal edges. Furthermore, in addition to gradient weighting of the directional derivatives, for some interfaces the attenuation coefficient values were added to the cost function. Several minor modifications, which included adaptation of the size of the used smoothing filters , were also introduced.

2. RETINAL LAYER SEGMENTATION

First, we briefly introduce the level sets framework (2.1), then we present solutions to deal with pathological changes in retinal structures that occur in eyes affected by dry AMD: the presence of additional interface (section 2.2) and adaptation of the initialization for the level set propagation (section 2.3) as well as the changes in the actual layer segmentation framework (section 2.4).

2.1 Introduction to loosely coupled level sets (LCLS) segmentation for retinal layer segmentation

The LCLS method consists of several steps, which include pre-processing, retinal feature detection, noise suppression and the actual layer segmentation. All interfaces between layers are segmented simultaneously based on a probabilistic framework which incorporates image data and prior knowledge about the retina. In this approach, every interface C_i is represented by its own level set function ϕ_i, which is propagated according to:

$$\frac{\partial \phi_i}{\partial t} = -\Delta t\big((\Pr(l_i|\mu) - 0.5) + \alpha\kappa_i + \beta\zeta_i\big)|\nabla\phi_i|\,, \qquad (1)$$

where $\Pr(l_i|\mu)$ is the probability of a voxel to belong to layer l_i, μ the attenuation coefficient of that voxel, and κ_i and ζ_i the interface-specific geometric regularization terms. The weights of different terms are denoted by α and β, while Δt is the time step. A more detailed description of the contribution of each individual term to the update of the level set function and processing steps can be found in our original paper[15]. Figure 2 shows an example of a segmentation result superimposed on an attenuation coefficient image of a healthy retina and includes some used OCT terminology.

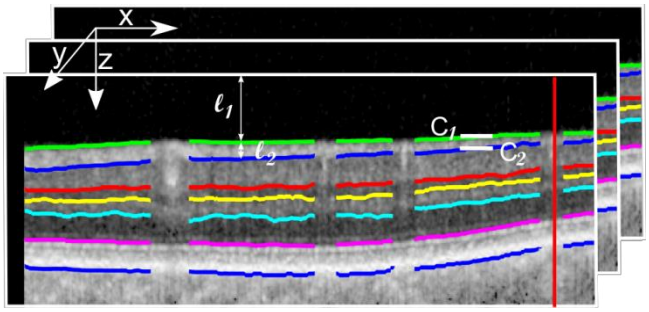

Figure 2. An example of the segmentation results obtained with our previously presented method on an attenuation coefficient B-scan of a healthy subject. The abbreviations of the layers are as follows (from top to bottom): vitreous, RNFL, GCL with IPL, INL, OPL, ONL, IS with RPE, choroid. The 3D coordinate system is indicated with arrows in the top left corner. The vertical red line indicates an A-line. Notations used for layers (l_1,l_2) and interfaces (C_1,C_2) in the segmentation framework are shown with white letters.

2.2 Bruch's membrane as an additional interface

As a result of the accumulation of extracellular material between Bruch's membrane and the RPE in eyes affected by dry AMD, Bruch's membrane is no longer adjacent to the RPE, but becomes separated and therefore visible. Since our previous approach did not include Bruch's membrane, an additional interface (C_8) that corresponds to this membrane is introduced in this extension. This interface is allowed to move arbitrarily close to the RPE boundary thereby creating an extra layer only if necessary to delineate the drusen. The resulting extra layer between the RPE and Bruch's membrane can be used to measure drusen volume and drusen height.

2.3 Initialization of interfaces

Propagation of the level set functions is done by simultaneously solving a set of partial differential equations that drive the current segmentation of the retinal interfaces to its minimum energy state. A rough initial indication of interfaces between the layers was found by using a minimum cost path search applied to individual B-scans. The general cost function was computed using the following expression:

$$C = \frac{(1-f(\pm g_z * I))+w_2 f(\pm I)}{w_1}, \quad (2)$$

where I is the image (positive sign) or its negative (negative sign) and g_z the Gaussian derivative in axial (z) direction favoring either bright-to-dark (negative sign) or dark-to-bright (positive sign) transitions. The function $f(x)$ was defined as $f(x) = \frac{x-\min(x)}{\max(x)-\min(x)}$. Finally, two weights ($w_1, w_2$) are used, where w_1 is associated with the prior knowledge about the shape of an interface and weight w_2 controls the contribution of attenuation coefficient values in the cost function. Attenuation coefficient values are included in the cost function to create a slight bias towards the thickest layers in the

Table 1. Summary of the weights used to initialize different interfaces. As cost is relative, only the ratio between the horizontal, vertical and diagonal costs is relevant. Thus, the cost for vertical edges is set to 1 and the cost for diagonal and horizontal edges was adjusted according to the expected shape of an interface.

Interface	***Weight for node connections (w_1)***		***Weight for att. coef. (w_2)***
	Horizontal	*Diagonal*	
Vitreous-RNFL	$w_1 = 1$	$w_1 = 1$	$w_2 = 0$
INL-OPL	$w_1 = \sqrt{2}$	$w_1 = 1$	$w_2 = 0.5$
OPL-ONL	$w_1 = \sqrt{2}$	$w_1 = 1$	$w_2 = 0.5$
IS boundary	$w_1 = 1/20$	$\sqrt{2}/20$	$w_2 = 0.7$
Bruch's membrane	$w_1 = 2$	$w_1 = 1$	$w_2 = 0.5$

region of interest (low values will have a low cost) which ensure that the shortest path search does not start to follow a neighboring interface of the same transition type. Furthermore, the negative of the image was used only for the INL – OPL interface. A summary of the weights used per interface is given in Table 1. Interfaces were initialized in a sequential manner. First, Bruch's membrane was initialized, followed by the inner and outer boundaries of the retina (the vitreous – RNFL interface and the IS boundary). Finally, the INL – OPL interface was segmented followed by the initialization of the OPL – ONL interface. The other interfaces were initialized at a spatially varying distance from the interfaces that were already segmented in accordance with previously reported layer thicknesses[18].

2.4 Retinal layer segmentation

After the initialization of interfaces (section 2.3), level set segmentation was performed on individual B-scans. As mentioned, an additional interface (C_8) was introduced, however, this interface was not propagated with the level set function, but remained fixed. Further, the RPE boundary was not allowed to propagate beyond Bruch's membrane. Other changes include adding maximal thickness priors for INL, OPL and ONL, which were set to 70, 60 and 120 µm, respectively. Additional minimal thickness prior was added for GCL+IPL and set to a value of 16 µm. The prior probability on attenuation coefficient was modelled as an error function with three parameters that controlled the threshold (μ_c), slope (σ) and magnitude (γ) of the prior probability. The slope and threshold of this prior probability were changed to values reported in Table 2. Further, similarly as in our previous approach, images were smoothed by using a steerable Gaussian filter[19] based on the orientation obtained from the 2D structure tensor[20]**.** However, the scales for computing the orientation and for smoothing the images differed from our original approach due to the drusen which disturb the morphology of the retina. The scale of the Gaussian derivatives to compute the gradient was set to 20 µm and the Gaussian tensor smoothing was set to be 80 µm along a B-scan and 20 µm across a B-scan. The filtering was performed only along the estimated orientation with a Gaussian filter of standard deviation 16 µm.

3. EXPERIMENTS

3.1 Data

Volumetric retinal OCT scans from patients suffering from dry AMD were obtained from a publicly available dataset[21]. Macular scans of five dry AMD patients (one eye per patient) were acquired with a Spectralis OCT system, however the raw OCT volume scans were not available. The exported datasets contained images in a tagged image file format. For more details on the used scan protocols, we refer the reader to Srinivasan et al.[21] Two B-scans with drusen were randomly selected from each volumetric scan for manual annotation. Manual segmentation was done on a slice-by-slice basis by a medical doctor using ITK-SNAP (publicly available at http://www.itksnap.org). The expert was asked to delineate the following interfaces: the vitreous - RNFL, the RNFL - GCL, the IPL - INL, the INL - OPL and the OPL - ONL, as well as the IS and RPE posterior boundary and Bruch's membrane.

Table 2. Parameter values for priors on attenuation coefficient . Magnitude (γ) remained the same as in our original paper and was set to a value of ±0.45.

	σ	$\mu_c(mm^{-1})$
Vitreous-RNFL	0.25	0.09
RNFL - GCL	2	0.86
IPL - INL	6	0.23
INL-OPL	6	0.23
OPL-ONL	6	0.23
IS boundary	6	0.64
RPE posterior boundary	1	5

3.2 Accuracy evaluation

A qualitative evaluation of the presented method on eyes affected by dry AMD was performed. The accuracy was determined by comparing the results of the automatic algorithm with the manually segmented data. For interfaces, the root-mean-square error (RMSE) and the mean-absolute deviation (MAD) were computed. The A-lines crossing the retinal vasculature were excluded in calculating the errors. For drusen, the Dice coefficient was used to assess the segmentation results.

Table 3 provides results on the accuracy of the automatic method. An error of 3.9 μm corresponded to one pixel along the A-lines. The accuracy of interface segmentation showed an RMSE ranging from 4.4 μm to 14.1 μm and an MAD ranging from 3.9 μm to 10.5 μm. The Dice coefficient was 0.81. Further, in Figure 3, an example of the automatic and a manual segmentation are depicted.

From the obtained segmentation one can create thickness maps of different layers. Examples of possible applications, such as drusen height and a thickness map of the ganglion cell complex (GCC; the combination of the RNFL, the GCL and the IPL) are shown in Figure 4. Drusen volume was shown to correlate with retinal sensitivity[8], whereas the GCC layer was shown to have a reduced thickness in eyes affected by AMD[4]. These maps were created by measuring the distance along every A-line between the RPE posterior boundary and Bruch's membrane and between the vitreous-RNFL interface and the GCL+IPL – INL interface, for drusen height and GCC thickness, respectively.

Table 3. Accuracy evaluation on eyes affected by dry AMD

	RMSE (μm)	**MAD** (μm)
Vitreous-RNFL	4.4	3.9
RNFL - GCL	*8.6*	5.9
IPL - INL	*7.5*	4.6
INL-OPL	10.1	6.5
OPL-ONL	9.6	6.1
IS boundary	8.0	3.9
RPE posterior boundary	*14.1*	10.5
Bruch's membrane	6.9	5.5

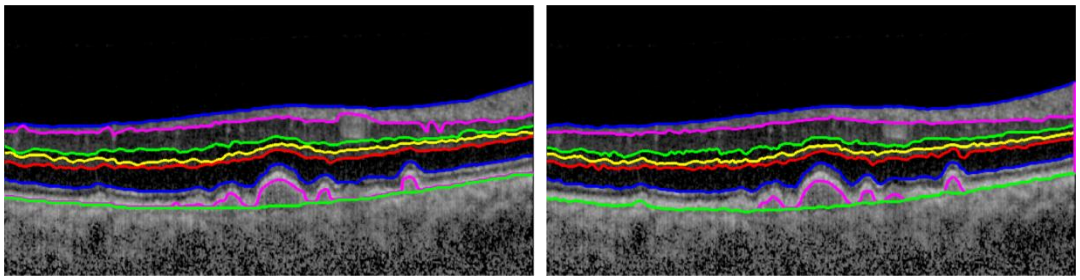

Figure 3. The automated (left) and a manual segmentation (right) result superimposed on the attenuation coefficient image of an eye affected with dry AMD.

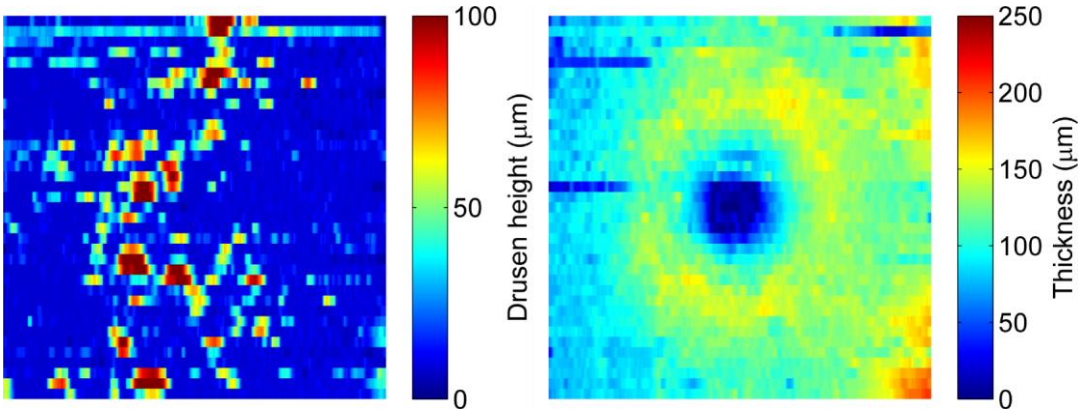

Figure 4. The generated spatial maps of drusen height (left) and the thickness of the GCC layer (right).

4. DISCUSSION

This paper presents a solution for the segmentation of interfaces between retinal layers and drusen in eyes affected by dry AMD based on a loosely coupled level sets approach. The solution, in addition to retinal layers, performs segmentation of Bruch membrane's and incorporates prior knowledge about the appearance of drusen into the initialization stage of the approach via a newly proposed cost function.

A good agreement was found between the segmentation performed manually by a medical doctor and those obtained from the automatic segmentation, with an MAD that varied between 3.9 – 10.5 μm (1 – 2.7 pixels) and a Dice coefficient of overlap of 0.81. Several other drusen segmentation approaches known in the literature reported overlap ratio for drusen segmentation of 67 %[11] and MAD for the interfaces that surround the drusen in the range of 3 - 6 μm[13] which is in a similar range as our results. In contrast to these approaches, our approach segmented and evaluated the segmentation of other retinal layers as well.

Overall, our method provides an accurate method to segment retinal layers and drusen. By performing segmentation of retinal layers in eyes affected by dry AMD, our proposed LCLS method becomes more generalized as it is also capable of handling topology disrupting diseases such as dry AMD. Future work includes extensions to other retinal diseases, such as central serous retinopathy.

Acknowledgements: The work was supported by Stichting Combined Ophthalmic Research Rotterdam, Stichting Glaucoomfonds, Stichting voor Ooglijders and ZonMw (grant number: 91212061).

REFERENCES

[1] Huang, D., Swanson, E., Lin, C., Schuman, J., Stinson, W., Chang, W., Hee, M., Flotte, T., Gregory, K., Puliafito, C., et al., "Optical coherence tomography", Science, 254, 1178–1181, (1991).
[2] West, S., Sommer, A. "Prevention of blindness and priorities for the future", Bulletin of the World Health Organization, 79, 244–248, (2001)
[3] Savastano, M. C., Minnella, A. M., Tamburrino, A., Giovinco, G., Ventre, S., Falsini, B., "Differential Vulnerability of Retinal Layers to Early Age-Related Macular Degeneration: Evidence by SD-OCT Segmentation Analysis", Investi gative Ophthalmology & Visual Science, 55, 560-566, (2014).
[4] Yenice, E., Sengun, A., Soyugelen Demirok, G., Turaclı, E., "Ganglion cell complex thickness in nonexudative age-related macular degeneration", Eye, (2015).

[5] Acton, J. H., Smith, R. T., Hood, D. C., Greenstein, V. C., "Relationship between Retinal Layer Thickness and the Visual Field in Early Age-Related Macular Degeneration", Investigative Ophthalmology & Visual Science, 53, 7618-7624, (2012).
[6] Wood, A., Binns, A., Margrain, T., Drexler, W., Povazay, B., Esmaeelpour, M., Sheen, N., "Retinal and Choroidal Thickness in Early Age-Related Macular Degeneration", American Journal of Ophthalmology, 152, 1030-1038, (2011).
[7] Hartmann, K. I., Bartsch, D.- U. G., Cheng, L., Kim, J. S., Gomez, M. L., Klein, H., Freeman, W. R., "Scanning laser ophthalmoscope imaging stabilized microperimetry in dry age-related macular degeneration", Retina, 31, 1323-1331, (2011).
[8] Sisternes, L. de, Simon, N., Tibshirani, R., Leng, T., Rubin, D. L., "Quantitative SD-OCT Imaging Biomarkers as Indicators of Age-Related Macular Degeneration Progression Predicting AMD Progression Using SD-OCT Features", Investigative Ophthalmology & Visual Science, 55, 7093-7103, (2014).
[9] Farsiu, S., Chiu, S. J., Izatt, J. A., Toth, C. A., "Fast detection and segmentation of drusen in retinal optical coherence tomography images", Proceedings of SPIE, 6844, (2008).
[10] Chiu, S. J., Izatt, J. A., O'Connell, R. V., Winter, K. P., Toth, C. A., Farsiu, S., "Validated Automatic Segmentation of AMD Pathology Including Drusen and Geographic Atrophy in SD-OCT Images", Investigative Ophthalmology & Visual Science, 53, 53-61, (2012).
[11] Chen, Q., Leng, T., Zheng, L., Kutzscher, L., Ma, J., de Sisternes, L., Rubin, D. L., "Automated drusen segmentation and quantification in SD-OCT images", Medical Image Analysis, 17, 1058-1072, (2013).
[12] Quellec, G., Lee, K., Dolejsi, M., Garvin, M. K., Abramoff, M. D., Sonka, M., "Three-dimensional analysis of retinal layer texture: identification of fluid-filled regions in SD-OCT of the macula", Medical Imaging, IEEE Transactions on, 29, 1321-1330, (2010).
[13] Dufour, P. A., Ceklic, L., Abdillahi, H., Schröder, S., de Dzanet, S., Wolf-Schnurrbusch, U., Kowal, J., "Graph-based multi-surface segmentation of OCT data using trained hard and soft constraints", Medical Imaging, IEEE Transactions on, 32, 531-543, (2012).
[14] Niu, S., Chen, Q., de Sisternes, L., Rubin, D. L., Zhang, W., Liu, Q., "Automated retinal layers segmentation in SD-OCT images using dual-gradient and spatial correlation smoothness constraint". Computers in Biology and Medicine, 54, 116-128, (2014).
[15] Novosel, J., Thepass, G., Lemij, H. G., de Boer J. F., Vermeer, K. A., van Vliet L. J., "Loosely coupled level sets for simultaneous 3D retinal layer segmentation in optical coherence tomography", Medical Image Anaylsis, (2015)
[16] Vermeer, K. A., Mo, J., Weda, J. J., Lemij, H. G., de Boer J. F., "Depth-resolved model-based reconstruction of attenuation coefficients in optical coherence tomography", Biomedical Optics Express, 5, 322-337, (2014).
[17] Dijkstra, E. W., "A note on two problems in connexion with graphs", Numerische Mathematik, 1, 269–271, (1959).
[18] Kafieh, R., Rabbani, H., Hajizadeh, F., Abramoff, M. D., Sonka, M., "Thickness Mapping of Eleven Retinal Layers Segmented Using the Diffusion Maps Method in Normal Eyes", Journal of Ophthalmology, (2015)
[19] Bakker, P., van Vliet, L.J., Verbeek, P.W., "Edge preserving orientation adaptive filtering", Computer Vision and Pattern Recognition, 1999. IEEE Computer Society Conference on., (1999)
[20] Knutsson, H., "Representing local structure using tensors", Proceedings 6th Scandinavian Conf. on Image Analysis, (1989)
[21] Srinivasan, P. P., Kim, L. A., Mettu, P. S., Cousins, S. W., Comer, G., M., Izatt, J., A., Farsiu S., "Fully automated detection of diabetic macular edema and dry age-related macular degeneration from optical coherence tomography images", Biomedical Optics Express, 5, 3568-3577, (2015)